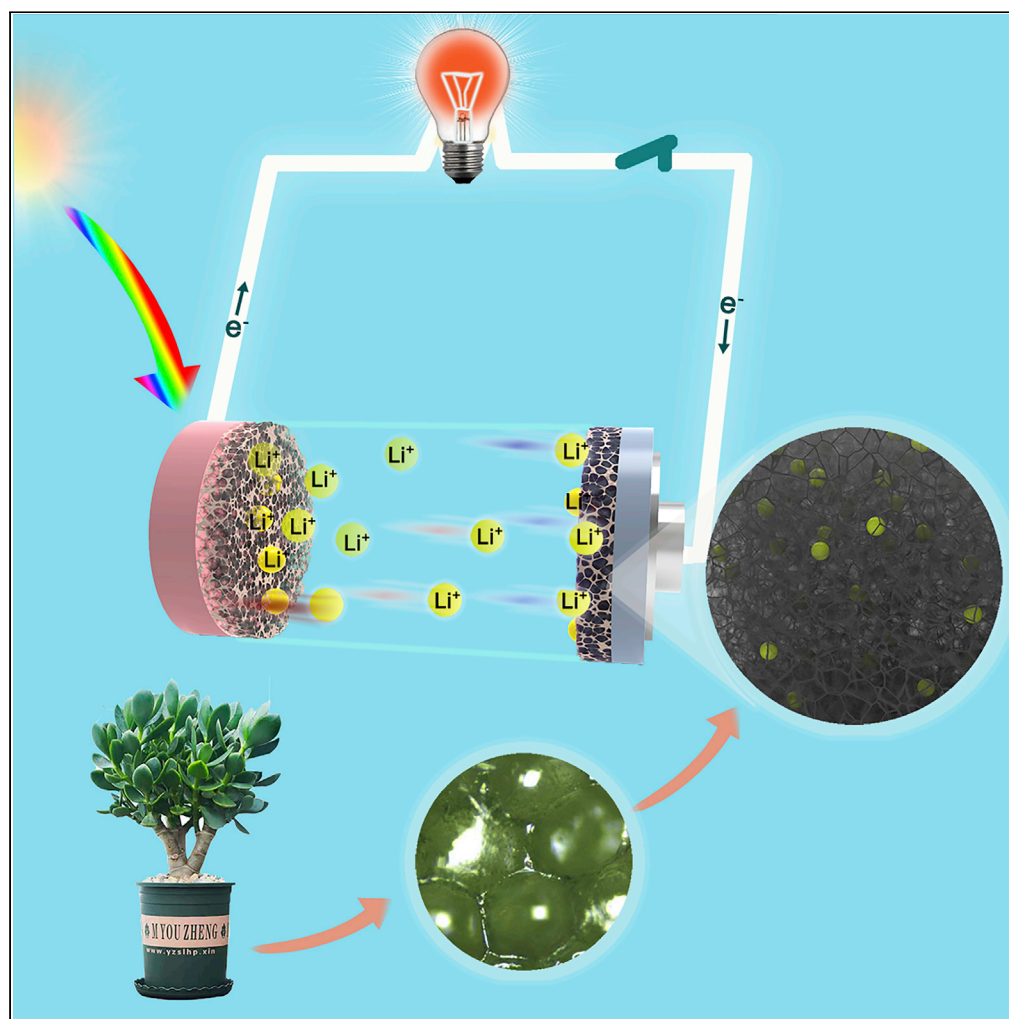


Article

Superior thermal-charging supercapacitors with bio-inspired electrodes of ultra-high surface areas



Tingting Meng,
Yimin Xuan,
Shengjie Peng

ywxuan@nuaa.edu.cn

Highlights

Graded porous carbon is prepared from succulents as initial raw materials.

The porous carbon presents a high specific surface area of up to $3188 \text{ m}^2 \text{ g}^{-1}$.

The NMR is utilized to characterize the superior ability of accommodating Li^+ .

The system with the porous carbon can generate a voltage of 565 mV at $\Delta T = 50^\circ \text{C}$.

Meng et al., iScience 25,
104113
April 15, 2022 © 2022 The
Author(s).
[https://doi.org/10.1016/
j.isci.2022.104113](https://doi.org/10.1016/j.isci.2022.104113)

Article

Superior thermal-charging supercapacitors with bio-inspired electrodes of ultra-high surface areas

Tingting Meng,¹ Yimin Xuan,^{1,3,*} and Shengjie Peng²

SUMMARY

High-performance thermally chargeable supercapacitors (TCS) greatly depend on the design of electrode materials. The unique features of succulents of absorbing water for sustaining their lives during long severe droughts imply that there exist vast spaces inside these plants, which inspires us of fabricating biomass-based electrodes by means of such succulents to develop highly efficient TCS. The optimized porous carbon prepared from succulents presents a high specific surface area of up to 3188 m² g⁻¹, resulting in the superior capability of accommodating a vast amount of ions and promising thermal charging performance. The TCS with this carbon electrode can generate an open-circuit voltage of 565 mV under a temperature difference of 50°C with a temperature coefficient as high as 11.1 mV K⁻¹. This article provides a new method for the preparation of porous carbon from biomass for the TCS system.

INTRODUCTION

Effective utilization of waste heat from industrial devices or solar energy is of great significance for alleviating energy shortages (Gao et al., 2017; Maye et al., 2020; Roychowdhury et al., 2019). There are currently two main forms of harvesting electric energy from low-grade waste heat, which are electrochemical thermocells and thermally chargeable supercapacitor (TCS) (Zhao et al., 2016). The former mainly relies on the entropy change in heat-sensitive redox pairs under temperature difference for thermoelectric conversion. Baughman et al. (Zhang et al., 2017) adopted ferri/ferrocyanide as electrolyte, which produced a power density of 12 W m⁻². Han et al. (2020) demonstrated a thermopower of 17.0 mV K⁻¹ by combining the thermodiffusion and thermogalvanic effects through the change in ion valence. The available redox pairs are relatively limited and this system can only generate electricity, and fail to store electricity. The TCS relies on the migration of ions under the temperature difference to form an electric double layer or ions intercalation on the surface of the cold electrode for thermoelectric conversion. Xuan et al. (Meng et al., 2021) combined the electric double layer with lithium ions intercalation, which can get a thermopower of 12.1 mV K⁻¹. TCS is in principle quite different from the current electric charging devices, which undergoes ion adsorption or ion intercalation reactions on the electrode surface during the charging process, which is exactly the opposite of the electrical charging process (Deyang, 2002; Lou et al., 2015). In addition, TCS is also different from traditional solid-state thermoelectric materials. The TCS system can store the electricity conveniently at the same time as the thermoelectric conversion, which is of practical significance to provide supplementary power in case of insufficient power supply.

The electric quantity of TCS is stored on the electrode surface in the form of surface charge, so the thermoelectric conversion behavior of TCS depends on the active surface area as well as the pore size distribution of the active materials (Ghosh et al., 2021; Pan et al., 2014; Wang et al., 2016b; Xiao et al., 2019). Carbon materials have received much attention due to the large effective surface areas, abundant interconnecting channels, and good electronic conductivity, benefiting the rapid adsorption and desorption of ions (Chang and Hu, 2019; Chmiola et al., 2006; Lin et al., 2015; Xie et al., 2021). In addition, the surface functional groups and crystal structure of the active electrodes are also extremely important for their capacity (Flouda et al., 2019; Hulicova-Jurcakova et al., 2009; Snoeyink and Weber, 1967; Tamás et al., 2006; Zhang et al., 2022). Therefore, it is of great importance to prepare activated carbon materials with plenty of interconnected pores and appropriate surface functional groups for TCS.

¹School of Energy and Power Engineering, Nanjing University of Aeronautics and Astronautics, Nanjing 210016, P. R. China

²College of Materials Science & Technology, Nanjing University of Aeronautics and Astronautics, Nanjing 210016, P. R. China

³Lead contact

*Correspondence: ymxuan@nuaa.edu.cn

<https://doi.org/10.1016/j.isci.2022.104113>



The sources of porous carbon materials are mainly from artificial manufacturing and natural plant carbonization. However, artificially manufactured porous carbon materials generally have a low specific surface area of about $1000 \text{ m}^2 \text{ g}^{-1}$, which limits the performance of TCS. In another regard, porous carbon materials derived from biomass have been demonstrated as a novel and important route to obtain low-cost and high-performance supercapacitor materials (Bai et al., 2020; Bi et al., 2019; Jin et al., 2018; Kim et al., 2020; Liu et al., 2019). Many kinds of biomass, such as egg white (Zhi et al., 2013), willow catkin (Li et al., 2016), garlic skins (Zhang et al., 2018), pine nut shells (Guan et al., 2019), coconut shells (Hulicova-Jurcakova et al., 2009) and brown seaweed (Kang et al., 2015), have been intensively studied as precursors of carbon materials. It has been illustrated that the porous carbon materials prepared by biomass have excellent electrochemical performance. Up to now, most of the activated carbon materials are prepared in the industry using coconut shell as the raw materials, but there are problems that affect ion transmission such as pore size mismatch with ionic sizes. Therefore, the key to improve the performance of TCS is to find precursors with the excellent structure for the preparation of high-performance carbon materials.

The water content of some succulent organs can get up to 90–95%. Succulent plants have plenty of parenchyma in their stems, leaves, and roots for storing water to defend the arid living environment (Heyduk, 2021), for which, succulent can sustain life for a long time even during drought. Moreover, succulents exhibit volume expansion in case water supply is sufficient (Ogburn and Edwards, 2010). Therefore, succulent tends to rapidly adsorb water molecules due to their good transfer channel between the cell walls (Grace, 2019), which inspire us to explore the possibility of whether such plants can be used to prepare carbonized materials for enhancing the intercalation and transportation of ions for thermal-electric conversion systems. In addition, succulents have higher oxygen content and a certain amount of nitrogen, which may inherit the oxygen and nitrogen to carbonized biological materials, enabling the improved electrochemical performance of the final carbon materials. Furthermore, succulent plants are widely distributed and easy to be manipulated by grafting, seeding, and root cutting, which largely lowers the price and facilitates further commercial applications. By integrating both aforementioned design rationales, it is believed that high electrochemical performance can be expected based on succulent-derived carbon materials.

Being inspired by the biological behaviors of succulents, in this article, the succulent plants (*Crassula arborescens* (Mill.) Willd.) are utilized as raw materials to prepare porous carbon materials with an alkaline activation process. Because of the unique channels in the leaves of succulent plants, how to maintain the basic structure of the leaves is a difficult problem in the preparation of carbon materials, which is also the key to ensure rapid ions transfer. In the experiment, we first use liquid nitrogen to keep the shape of the leaves, and then utilize freeze-drying technology to retain the internal structure of the leaves to the greatest extent. The optimized succulent-derived porous carbon presents an ultra-high specific surface area of $3188 \text{ m}^2 \text{ g}^{-1}$ and abundant micro-porous and meso-porous structures. This carbon electrode material has excellent cycle stability (capacitance retention rate is 94% after 8000 cycles in 1 M H_2SO_4 solution). In addition, the application of this biomass electrode in the field of TCS is investigated experimentally (Han et al., 2020; Meng and Xuan, 2020). The thermally chargeable system based on this electrode can generate an open-circuit voltage of 565 mV under a temperature difference of 50°C , and the temperature coefficient is as high as 11.1 mV K^{-1} . Besides, Li_2SO_4 is used as an electrolyte for NMR for the first time, and the adsorption capacity of Li^+ of different carbon electrodes after the completion of charging is measured. Based on sustainable succulent plant materials, simple synthesis process and excellent electrochemical performance, the strategy proposed here provides a new research direction for the preparation of TCS electrode materials.

RESULTS

The principle and characteristic analysis of thermally chargeable supercapacitors

TCS system can utilize the waste heat from sunlight or factory to carry out thermoelectric conversion under temperature difference. The lithium ion moves to the cold electrode firstly to form an electric double layer on the electrode surface or embedded into the electrode when the temperature difference is established, as shown in Figure 1. The electric potentials of the electrodes are not identical and there exists a potential difference between them, so that the electric charges are stored on the electrode surfaces. The electrons migrate to the hot electrode to complete the discharge process when the external circuit is connected to supplement the lack of electricity. Electrodes with ultra-high specific surface areas can store more charges during a thermally charging process. Therefore, the specific surface area and pore size

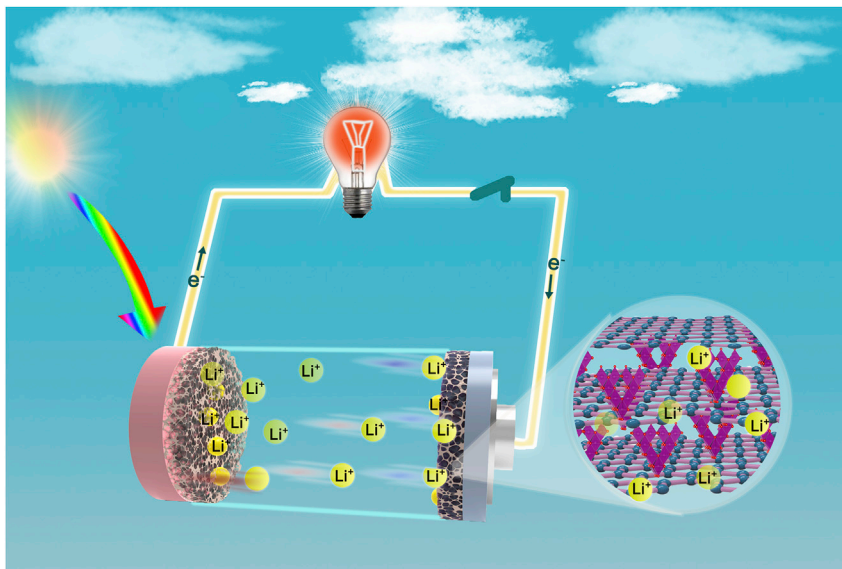


Figure 1. Schematic diagram of TCS

See also [Figure S1](#).

distribution of electrode active materials are very important for the thermal charging performance of the TCS system.

Synthesis of the C-4-700

Four types of hierarchical porous carbon materials are prepared from succulents as initial raw materials by tuning the ratio of carbon powder and KOH, referred to C-700, C-2-700, C-3-700, C-4-700, and C-4.5-700, which refers to the cases that the ratio of KOH to carbon powder is selected to be 2:1, 3:1, 4:1, and 4.5:1, respectively. Especially, C-700 means without being activated. Here the carbonization temperature is 700°C. For example, the preparation flow chart of biomass-derived porous carbon material, C-4-700 is shown in [Figure 2](#). The cells in fresh succulent plant leaves are plump due to being full of water and there are well-developed channels among these cells. Such phenomena hint the potential features that this unique structure not only ensures the ion transport but also facilitates the entry of KOH in the activation process. The texture of dried succulent plant leaves obtained by freeze-drying is similar to that of sponges, and retains the internal cell structure and ion channels of fresh succulents. After the two important processes of carbonization and activation, the crushed fleshy leaves can be transformed into porous carbon materials with well-defined pores. During the activation process, the introduction of the activator KOH can remarkably improve the pore size and surface area of the carbon material, as well as generate functional groups that can improve the electrochemical performance of the carbon material. As shown in [Figure 2](#), the pore morphology of the carbon material after activation by KOH is honeycomb-shaped, consistent with the initial cell structure.

Morphology and structure characterization

The microstructure and morphology of C-4-700 are characterized by scanning electron microscope (SEM) and transmission electron microscope (TEM). It can be observed from [Figure 3A](#) that the surface of C-4-700 presents an interconnected structure, which is attributed to the activation treatment of KOH. The material is constructed by numerous open large pores, indicating that the materials form a layered structure connected by macro-, meso- and micro-pores, which is very important to affect the supercapacitive performance. The macro- and meso-pores are responsible for the storage sites of the electrolyte, thereby reducing the diffusion distance of ions. Meanwhile, the existence of multi-level pore structure is able to produce a larger effective surface area, so as to effectively improve the electrochemical performance of carbon materials. [Figures 3C](#) and [3D](#) indicate that there are abundant macro-, meso-, and micro-pores in the material. In particular, [Figure 3C](#) illustrates that the cell architecture of succulent plant leaves is well preserved to a certain extent during the activation process, ensuring the hierarchical porous structure of the materials.

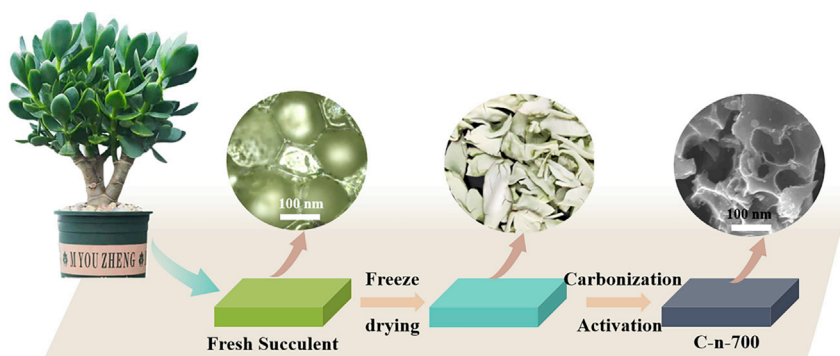


Figure 2. Schematic of the preparation process of biomass-derived porous carbon material

X-ray diffraction (XRD) spectra, Raman spectrum, and X-ray photoelectric spectroscopy (XPS) are utilized to investigate the structure of the porous carbon materials. As shown in Figure 4A, two broad diffraction peaks at $2\theta = 25$ and 43° can be observed for C-700, corresponding to the (002) and (100) lattice plane of disordered carbon and graphitic carbon, respectively. In particular, compared with C-700, the peak intensity of the activated carbon material at $2\theta = 25^\circ$ gradually becomes weak and finally disappears with the increase of activator KOH ratio, illustrating that alkaline activation could disorder the structure of obtained porous carbon, which is conducive to the increase of the specific surface area of the carbon materials. Raman spectroscopy can be further utilized to characterize the degree of graphitization of the samples. These four carbon materials all have two obvious peaks located at ca. 1340 cm^{-1} (D band) and 1580 cm^{-1} (G band) as shown in Figure 4B. In general, the defects and disorder degree of carbon materials are related to the D band, while the structural integrity of graphite is correlated with the G band. The intensity of G band of the tested samples is greater than that of D band, signifying that the materials are all part of graphitized carbon materials (Wang et al., 2016a). The disorder degree of carbon materials is evaluated by the I_D/I_G obtained by Raman spectroscopy (Hu et al., 2016). Among them, the I_D/I_G value of C-4-700 amounts to 0.993 and is larger than those of C-3-700 (0.987), C-2-700 (0.929), and C-700 (0.907), which demonstrates that the enhancement of the activation increases the disordered structure in the materials, which is consistent with the XRD results.

XPS examinations are further performed to obtain more information about the surface functional groups of these carbon materials. Figure 4C shows the XPS full spectrum comparison chart of C-700 and C-4-700. The characteristic lines of C 1s, N 1s, and O 1s appear in the full spectrum of the two materials, and the C-4-700 contains more abundant nitrogen (2.64%) and oxygen (17.58%). The presence of N and O not only improves the conductivity of the material but also facilitates the formation of pseudo-specific capacitance. Therefore, the activated carbon material has more excellent electrochemical performance. The C 1s high-resolution spectrum of C-4-700 is shown in Figure 4E. It is composed of four peaks, which C=C/C-C (284.8 eV), C-N (258.8 eV), C-O (286.9 eV), and O=C-O (289.3 eV) (Li et al., 2012). In the O 1s spectrum, as shown in Figure 3D, there are three typical oxygen-containing functional groups, referred to the hydroxyl functional group C=O (531.0 eV), the phenol or ether functional group C-OH or C-O-C (532.4 eV) as well as carboxyl functional group O=C-O (535.1 eV) (Ming et al., 2017). The presence of these oxygen-containing functional groups can effectively improve the wetting property of these active materials and thereby improve the capacitance (Guo et al., 2014; Li et al., 2015). In addition, C-4-700 also has a more obvious N 1s peak, which can be simulated as a single peak, chiro/pyridone N (N-5, 399.5 eV). According to the literature reports, the electrode electrochemical reaction mainly occurs at the active site of N-5, which provides abundant pseudocapacitance (Chen et al., 2016). Therefore, the existence of this peak indicates that the prepared bio-carbon material can be beneficial to forming Faraday pseudocapacitance and then increase overall capacity. Therefore, C-4-700 is expected to have superior electrochemical capacity and performance compared to C-700.

Pore structures of C-700, C-4-700, and C-4.5-700 are analyzed by the N_2 adsorption and desorption method, which are shown in Figure S2. Obviously, the absorption curves of all these three samples rise sharply under low pressure ($P/P_0 = 0.0\text{--}0.1$), which indicates that the material has a strong force with nitrogen. At the medium pressure ($P/P_0 = 0.3\text{--}0.8$), due to the effect of KOH activation, the slope of the

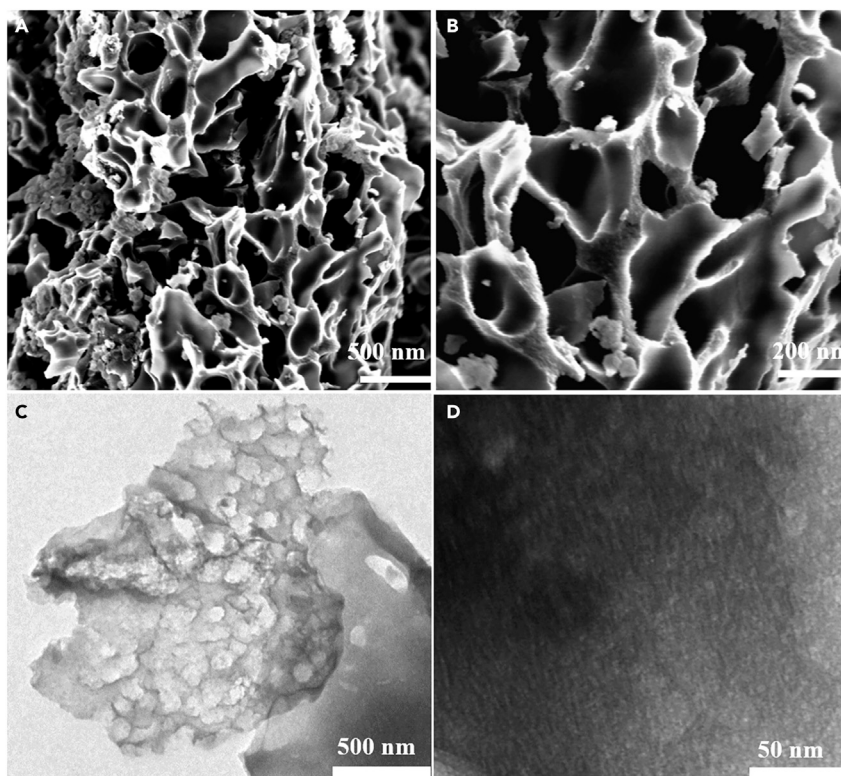


Figure 3. Physical characterization of C-4-700

(A and B) SEM images of C-4-700.

(C) TEM images of C-4-700.

(D) HRTEM images of C-4-700.

See also [Figure S3](#).

medium pressure curve of C-4-700 is larger than that of the C-700, indicating a larger number of mesopores in C-4-700. The detailed parameters for porous carbon materials are summarized in [Table 1](#). It is noted that when the carbonization temperature is 700°C and the ratio of activator to carbon powder is 4:1, the specific surface area and the pore volume can reach 3188 m² g⁻¹ and 1.90 cm³ g⁻¹, respectively, with an average pore diameter of 2.30 nm. The appropriate pore size is conducive to the entry of ions, and the large pore volume provides enough space for ions, facilitating the enhancement of the electrochemical performance. At the same time, we explored the specific surface area of succulent plants in different growth periods after treatment. Interestingly, under the same treatment conditions, the plants with longer growth periods exhibit higher specific surface areas after carbonization (as shown in [Figure S4](#)).

The electrochemical performance of C-4-700

In order to estimate the performance of these different porous carbon materials, the electrodes prepared from these carbon materials were adopted as the working electrodes in a three-electrode system in 1 M H₂SO₄, while platinum and calomel electrodes work as the counter and reference electrodes, respectively. [Figures 5A](#) and [5B](#) illustrate the cyclic voltammetry curves of these samples at 100 mV s⁻¹ and C-4-700 at different scan rates of 20 mV s⁻¹, 50 mV s⁻¹, 100 mV s⁻¹, and 200 mV s⁻¹. The CV curves of these electrodes show the typical rectangular shape of the electric double layer, and C-4-700 shows a larger and more perfect rectangle at this scanning rate, indicating that the material has the highest capacitance. Even at a high scan rate, C-4-700 can still maintain a good rectangular shape, indicating that the material has good magnification performance. [Figures 5C](#) and [5D](#) show the constant current charge and discharge test results of all samples at a current density of 1A g⁻¹ and C-4-700 at different current densities of 1A g⁻¹, 2A g⁻¹, and 5A g⁻¹, respectively. The galvanostatic charge and discharge (GCD) curves all show slightly deformed symmetrical triangles at current densities of 1, 2, and 5A g⁻¹, which prove the excellent

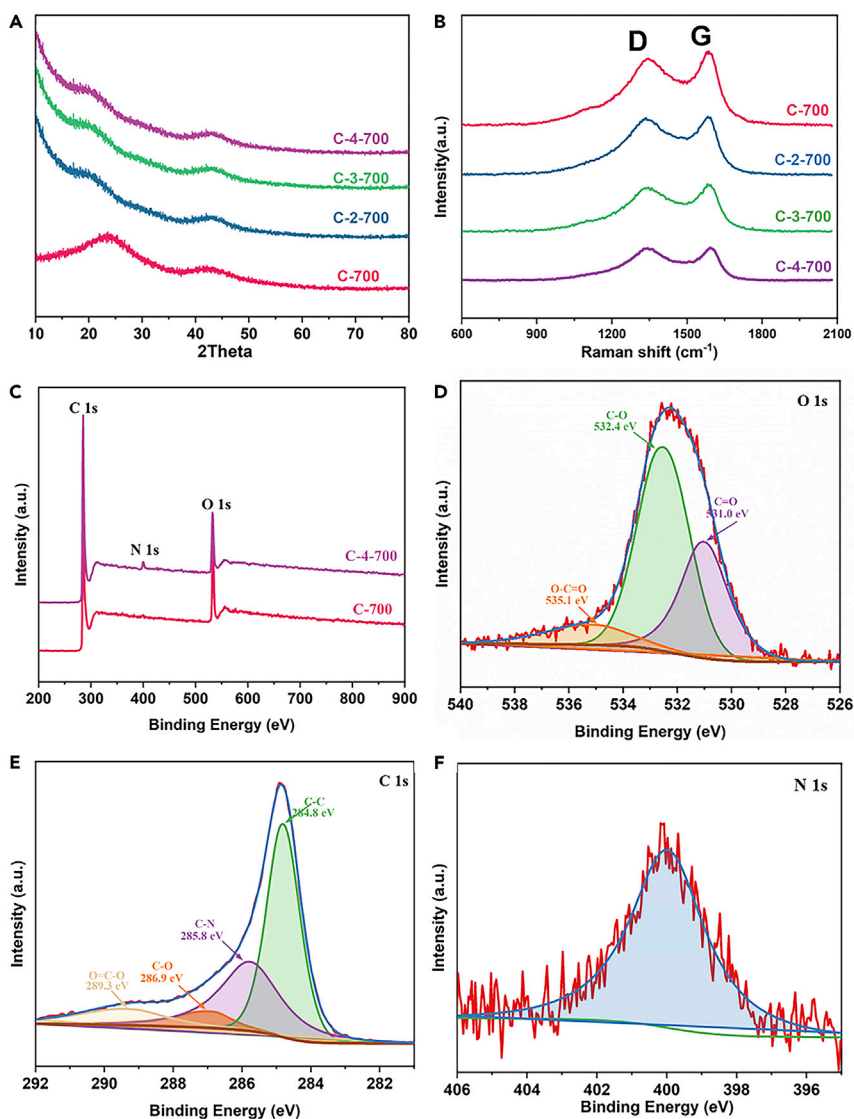


Figure 4. Characterization of porous carbon materials

(A) XRD patterns of C-700, C-2-700, C-3-700 and C-4-700.

(B) Raman spectrum of C-700, C-2-700, C-3-700 and C-4-700.

(C–F) (C) XPS spectra of C-700 and C-4-700, as well as the high-resolution spectra of (D) O 1s, (E) C 1s, and (F) N 1s of C-4-700.

charge storage performance of the C-4-700. In addition, the curve is distorted due to the pseudocapacitance generated by the Faraday reaction of the functional group on the sample surface. There is almost no voltage drop at the beginning of the discharge, indicating that the internal resistance of the electrode material is relatively small. According to the discharging phase, the weight capacitance of the electrode material is calculated to be 117.8 F g^{-1} .

In order to further evaluate the electrochemical performance of C-4-700, electrochemical impedance spectroscopy (EIS) test is carried out in an open-circuit state with the frequency range from 0.01 Hz to 10 kHz on these electrodes (as shown in Figure 6A). As a result, all samples show approximately straight lines and small curved arcs in the low-frequency and high-frequency regions, respectively, which represent a rational capacitor behavior. The larger slope of the EIS curve indicates faster ions diffusion, while the semicircular arc means the charge transfer resistance. The results show that the slope of the straight line C-4-700 is significantly higher than that of C-2-700 and C-3-700, indicating that the activated material has a developed

Table 1. BET surface area and pore structure characterization parameters of different carbon materials^a

Sample	S_{BET} ($\text{m}^2 \text{g}^{-1}$)	S_{micro} ($\text{m}^2 \text{g}^{-1}$)	V_{tot} ($\text{cm}^3 \text{g}^{-1}$)	V_{micro} ($\text{cm}^3 \text{g}^{-1}$)	D_{aver} (nm)
C-700	942	740	0.64	0.38	1.9
C-2-700	1491	1221	0.70	0.61	1.98
C-3-700	2463	1104	1.30	0.48	2.11
C-4-700	3188	1648	1.90	0.60	2.30
C-4.5-700	2418	1103	1.23	0.46	2.10

See also [Figures S2](#) and [S4](#).

^awhere: S_{BET} means a specific surface area determined by the BET method, S_{micro} means micropore surface area from the t-plot. V_{tot} and V_{micro} mean the total pore volume and micropore volume from the t-plot, respectively. D_{aver} means the adsorption average pore diameter.

ion channel so as to transfer ions faster. All the results show the C-4-700 material has a smaller contact resistance and charge transfer resistance.

To evaluate the electrochemical stability of C-4-700, a cycle stability test is conducted at a current density of 2 A g^{-1} , and the result is shown in [Figure 6B](#). The electrode material has a capacity retention rate of 94% after 8000 cycles, indicating good cycle stability. The above electrochemical tests show that the C-4-700 material with an ultra-high specific surface area and an appropriate porosity exhibits excellent electrochemical performance, indicating the feasibility of succulents in the preparation of porous carbon materials.

The performances of these supercapacitors based on bio-inspired carbon materials are evaluated in a two-electrode system with an electrolyte of $1 \text{ M H}_2\text{SO}_4$ and illustrated in [Figure 7](#). [Figure 7A](#) shows the

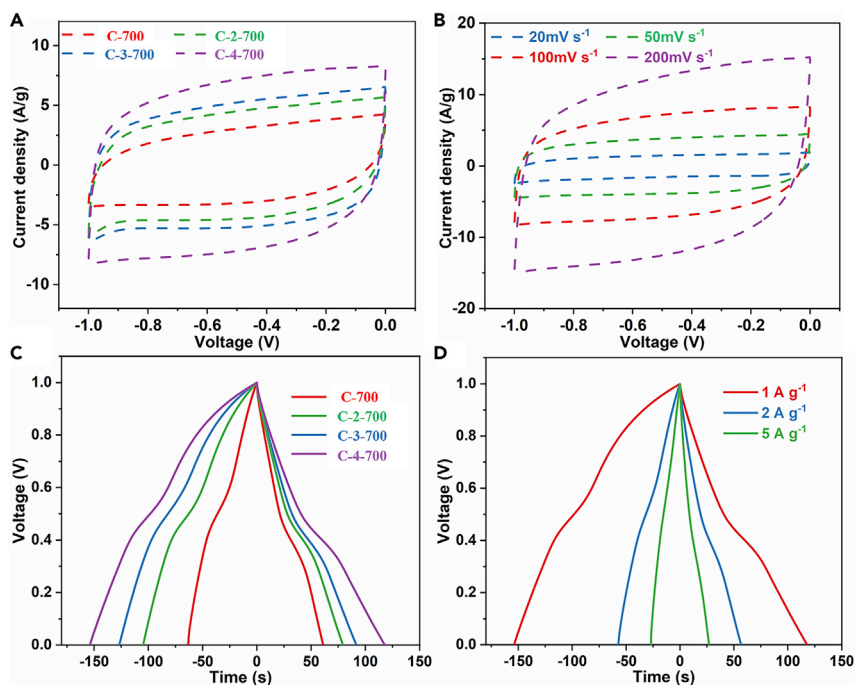


Figure 5. Tests results of the three-electrode system

(A) CV curves of different carbon materials under the same test conditions.

(B and C) (B) CV curves of C-4-700 at different scan rates, (C) GCD curves of different carbon materials under the same test conditions.

(D) GCD curves of C-4-700 at different current densities.

See also [Figure S6](#).

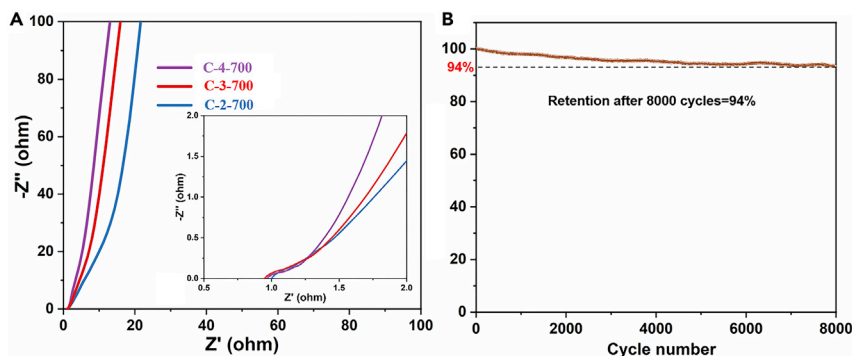


Figure 6. Measurement of electrochemical properties of porous carbon materials

(A) Nyquist plots of C-2-700, C-3-700, and C-4-700, (B) Cycling stability of the C-4-700.

See also [Figure S5](#).

CV curves of several carbon supercapacitors at a scanning rate of 100 mV s^{-1} . Obviously, all these CV curves show an approximate rectangular shape, indicating the behavior of the dominant electric double-layer capacitance. Obviously, the CV loop area of C-4-700 is much larger than that of the other three samples, which represent the highest capacitance. Meanwhile, the CV curves of C-4-700 at different scanning rates are measured to verify the magnification performance of the electrode (as shown in [Figure 7B](#)). The results show that the CV Curve maintains a perfect rectangular shape even at the scanning rate of up to 200 mV s^{-1} . Then the GCD distributions of several electrodes at a current density of 1 A g^{-1} are recorded. As shown in [Figure 7C](#), all curves are in a typical triangular shape, with good capacitance and

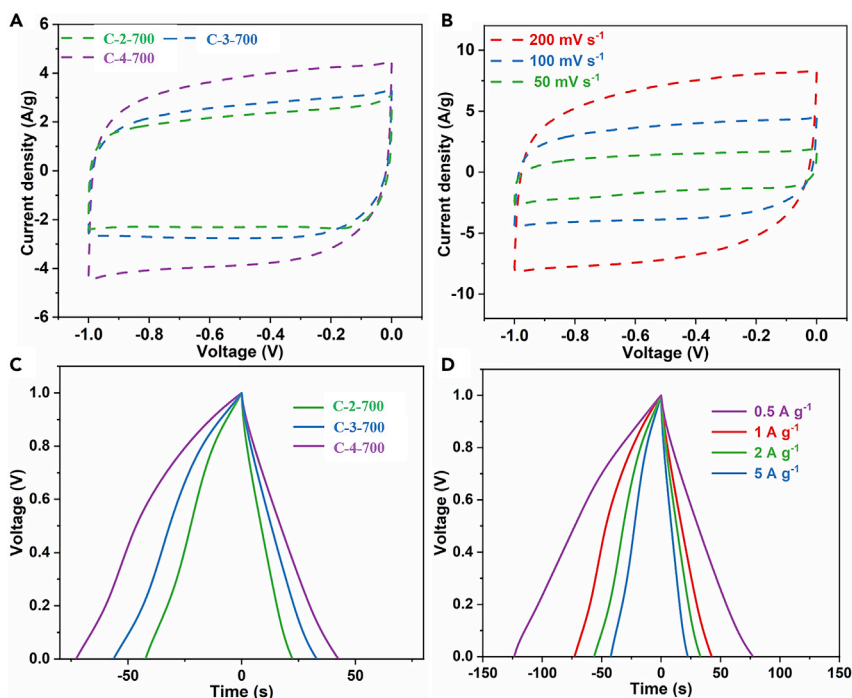


Figure 7. Tests results of the two-electrode system

(A) CV curves of different carbon materials under the same test conditions.

(B) CV curves of C-4-700 at different scan rates.

(C) GCD curves of different carbon materials under the same test conditions.

(D) GCD curves of C-4-700 at different current densities.

See also [Figures S7](#) and [S8](#).

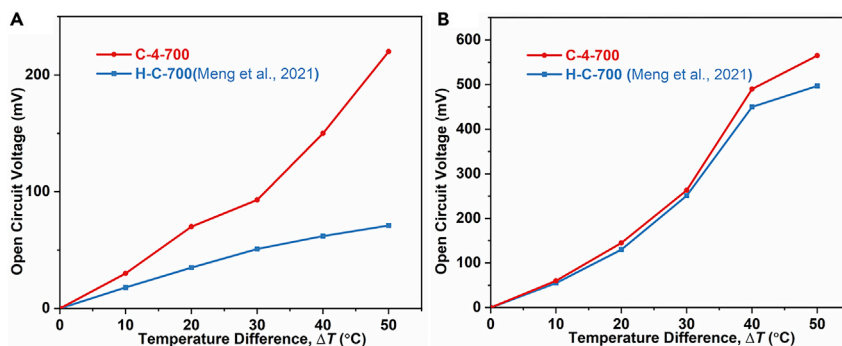


Figure 8. The thermal charging performance of C-4-700 porous carbon material

(A) The thermal charging performance of C-4-700 in electric double-layer thermally chargeable supercapacitor.

(B) The thermal charging performance of C-4-700 in hybrid thermally chargeable supercapacitor system and its comparison with Ref. 7.

electrochemical reversibility. When the current density is adjusted to 1 A g^{-1} in a run of experiment, specifically, the large specific capacitance of 170 F g^{-1} can be provided (as shown in Figure 7D). More experiments illustrate that the supercapacitors composed of the bio-carbon materials electrodes prepared from the succulents with longer growth periods exhibit better electrochemical performance (as shown in Figures S6 and S7).

The thermal charging performance of C-4-700

In order to simultaneously explore the application of C-4-700 porous carbon material in TCS, C-4-700 electrodes are employed as both positive and negative electrodes and Li_2SO_4 is adopted as electrolyte. One side is heated to an elevated temperature by a heating plane, while the other is maintained at 25°C through a circulating water bath. By adjusting the temperature of the hot electrode, the open-circuit voltage of the two sides of the system at the temperature difference of 10°C , 20°C , 30°C , 40°C , and 50°C , is recorded by a data collector, which is compared with the thermal charging performance of peanut shell porous carbon (H-C-700) electrode (Meng et al., 2021) used in reference 7. As shown in Figure 8A, when the temperature difference is 50°C , the open-circuit voltage of the electric double layer TCS system based on C-4-700 electrode can reach 220 mV , and the temperature coefficient is 4.4 mV K^{-1} , which is much larger than the system based on H-C-700 electrode. It may benefit from the ultra-high specific surface area of C-4-700 carbon material. In order to further study the thermal charging performance of the C-4-700 electrode, the C-4-700 electrode is employed as the hot side electrode, while the mixed electrode of lithium manganate, graphene, and carbon nanotube is utilized as the cold side electrode. By changing the temperature differences between the hot and cold electrodes, the application of the C-4-700 electrode in the hybrid TCS is explored. Compared with the H-C-700 system, as shown in Figure 8B, the C-4-700 system exhibits an open-circuit voltage of 565 mV under a temperature difference of 50°C , and the temperature coefficient is as high as 11.1 mV K^{-1} , which is still higher than that of H-C-700 electrode. Therefore, C-4-700 porous carbon material also has good performance for the application to TCS due to its ultra-high specific surface area.

The possible distribution of Li^+ in the porous electrode is shown in Figure 9A when the thermal charging process is completed. Due to the ultra-high specific surface area and wide pore size distribution of the porous electrode, more Li^+ will enter the electrode and adsorb on the porous surface, as shown in the local enlarged view of Figure 9A. NMR is carried out to further explain the number of lithium ions in the porous electrode. The ^7Li -NMR test is performed at the two electrodes used in Figures 8A and 8B (labeled 1 and 2, respectively), which are acquired on a 600 spectrometer. The charged electrode is freeze-dried immediately, which can effectively bind the adsorbed Li^+ to the electrode surface. The adsorption quantity of Li^+ in the two electrodes under the same test conditions is obtained, as shown in Figure 9 (Figure 9C is a magnification of Figure 9B at 0 ppm). The spectra of these samples show the main signal at about 0 ppm (the other signals are spinning sidebands). The static ^7Li NMR spectrum of these electrodes, Figure 9B, presents a clear difference in line width [40]. The C-4-700 resonance is significantly narrower, which is a result of the narrow mobility induced by Li ions, while the smaller mobility

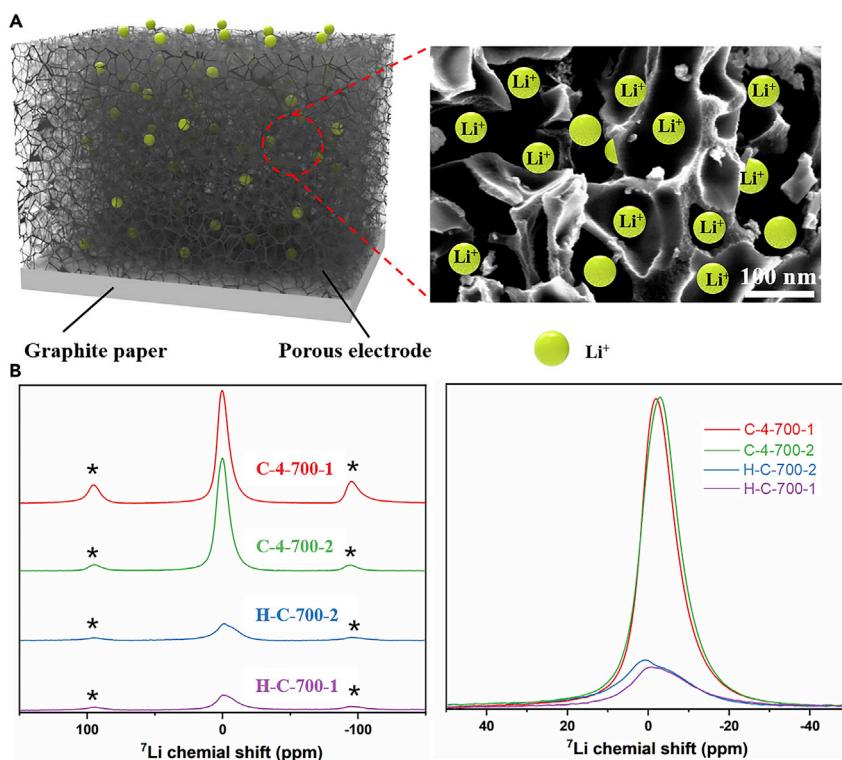


Figure 9. Distribution of Li^+ in electrodes after the thermal charging process

(A) Possible distribution state of lithium ion in porous electrode.

(B) ^7Li -NMR spectra of electrodes used in Figures 7A and 7B.

in H-C-700 results in a broad resonance. It is proved that the pore size distribution of C-4-700 is more favorable for the migration of ions. Comparing the spectra of C-4-700 and H-C-700 at the same time, C-4-700 shows a higher peak area, which represents a larger ion adsorption capacity and a more beneficial thermal charging behavior. The peaks of C-4-700-1 and two are slightly shifted, which may be caused by different cathode materials utilized.

The results of NMR are consistent with the experimental data of thermal charging tests, which further explains the reason why C-4-700 electrodes show better performance in the TCS system. Besides, it is more strongly explained that the specific surface area and pore size distribution of the active material are very important to improve the performance of the TCS system. The appropriate pore size is more conducive to the entry of ions, and the ultra-high specific surface area provides more adsorption sites for ions. Therefore, the C-4-700 electrodes tend to have excellent thermal charging performance.

DISCUSSION

In summary, we have successfully developed biocarbon-based electrodes with ultra-high specific surface areas being inspired by superior ability of succulents of accommodating water. The specific surface area of such porous electrodes prepared from succulents can amount to $3188 \text{ m}^2 \text{ g}^{-1}$. Due to the synergistic effect of the ultra-high specific surface area of the porous electrode and the functional group of N and O elements, this type of biomass porous carbon material exhibits good electrochemical performance. The experiment has indicated that the capacitance retention rate can reach 94% after 8000 cycles at 2 A g^{-1} . We have verified the application feasibility of this electrode to thermal charging through a series of experiments conducted with a thermally charging device made of the above-mentioned biocarbon porous electrodes. The hybrid TCS system assembled with this electrode has excellent thermoelectric conversion performance, which can generate an open-circuit voltage of 565 mV at a temperature difference of 50°C with a temperature coefficient as high as 11.1 mV K^{-1} . Due to the easy availability and simple synthesis process, this biomass porous carbon material

has great potential in batteries and thermal charging fields. Furthermore, this work also provides a new development direction for biomass in the field of carbon material preparation.

Limitations of the study

By adjusting the carbonization temperature and activation degree, we obtained porous carbon materials based on succulents with ultra-high specific surface areas. Besides, we compared succulents of different growth ages and found that the carbon materials obtained after the treatment of succulents with higher age tend to have a larger specific surface area. However, microscopic characterization is required to explain this phenomenon. In addition, more characterization is needed to understand the migration properties of ions in the pores, which is also the work we need to continue in the future.

STAR★METHODS

Detailed methods are provided in the online version of this paper and include the following:

- KEY RESOURCES TABLE
- RESOURCE AVAILABILITY
 - Lead contact
 - Materials availability
 - Date and code availability
- EXPERIMENTAL MODEL AND SUBJECT DETAILS
- METHOD DETAILS
 - Synthesis of porous carbon materials
 - Material characterizations
 - Electrochemical measurements of electrodes
- QUANTIFICATION AND STATISTICAL ANALYSIS

SUPPLEMENTAL INFORMATION

Supplemental information can be found online at <https://doi.org/10.1016/j.isci.2022.104113>.

ACKNOWLEDGMENT

This work was financially supported by the Basic Science Center Program for Ordered Energy Conversion of the National Natural Science Foundation of China (No.51888103) and Natural Science Foundation of Jiangsu Province (No. BK20202008).

AUTHOR CONTRIBUTIONS

Tingting Meng: Conceptualization, Methodology, Validation, Investigation, Writing - original draft, Writing - review & editing, Visualization. Yimin Xuan: Conceptualization, Supervision, Resources, Writing - review & editing, Project administration, Funding acquisition. Shengjie Peng: Writing - review & editing.

DECLARATION OF INTERESTS

The authors declare no conflict of interest.

Received: January 26, 2022

Revised: March 2, 2022

Accepted: March 14, 2022

Published: April 15, 2022

REFERENCES

- Bai, Q., Li, H., Zhang, L., Li, C., and Uyama, H. (2020). Flexible solid-state supercapacitors derived from biomass Konjac/Polyacrylonitrile-based nitrogen-doped porous carbon. *ACS Appl. Mater. Inter.* 12, 55913–55925. <https://doi.org/10.1021/acsami.0c16752>.
- Bi, Z., Kong, Q., Cao, Y., Sun, G., Su, F., Wei, X., Li, X., Ahmad, A., Xie, L., and Chen, C.-M. (2019). Biomass-derived porous carbon materials with different dimensions for supercapacitor electrodes: a review. *J. Mater. Chem. A* 7, 16028–16045. <https://doi.org/10.1039/C9TA04436A>.
- Chang, L., and Hu, Y.H. (2019). Breakthroughs in designing commercial-level mass-loading graphene electrodes for electrochemical double-layer capacitors. *Matter* 1, 596–620. <https://doi.org/10.1016/j.matt.2019.06.016>.
- Chen, J., Han, Y., Kong, X., Deng, X., and Ji, H. (2016). The origin of improved electrical double-layer capacitance by inclusion of topological defects and dopants in graphene for supercapacitors. *Angew. Chem. Int. Ed.* 55,

- 13822–13827. <https://doi.org/10.1002/anie.201605926>.
- Chmiola, J., Yushin, G., Gogotsi, Y., Portet, C., Simon, P., and Taberna, P. (2006). Anomalous increase in carbon capacitance at pore sizes less than 1 nanometer. *Science* 313, 1760–1763. <https://doi.org/10.1126/science.1132195>.
- Deyang, Q. (2002). Studies of the activated carbons used in double-layer supercapacitors. *J. Power Sourc.* 109, 403–411. [https://doi.org/10.1016/S0378-7753\(02\)00108-8](https://doi.org/10.1016/S0378-7753(02)00108-8).
- Flouda, P., Shah, S.A., Lagoudas, D.C., Green, M.J., and Lutkenhaus, J.L. (2019). Highly multifunctional dopamine-functionalized reduced graphene oxide supercapacitors. *Matter* 1, 1532–1546. <https://doi.org/10.1016/j.matt.2019.09.017>.
- Gao, C., Lee, S.W., and Yang, Y. (2017). Thermally regenerative electrochemical cycle for low-grade heat harvesting. *ACS Energy Lett.* 2, 2326–2334. <https://doi.org/10.1021/acsenerylett.7b00568>.
- Ghosh, S., Rao, G.R., and Thomas, T. (2021). Machine learning-based prediction of supercapacitor performance for a novel electrode material: Cerium oxynitride. *Energy Storage Mater.* 40, 426–438. <https://doi.org/10.1016/j.ensm.2021.05.024>.
- Grace, O.M. (2019). Succulent plant diversity as natural capital. *Plants People Planet.* 1, 336–345. <https://doi.org/10.1002/ppp3.25>.
- Guan, L., Pan, L., Peng, T., Gao, C., Zhao, W., Yang, Z., Hu, H., and Wu, M. (2019). Synthesis of biomass-derived nitrogen-doped porous carbon nanosheets for high-performance supercapacitors. *ACS Sustainable Chem. Eng.* 7, 8405–8412. <https://doi.org/10.1021/acssuschemeng.9b00050>.
- Guo, C., Na, L., Ji, L., Li, Y., Yang, X., Yun, L., and Tu, Y. (2014). N- and O-doped carbonaceous nanotubes from polypyrrole for potential application in high-performance capacitance. *J. Power Sourc.* 247, 660–666. <https://doi.org/10.1016/j.jpowsour.2013.09.014>.
- Han, C.-G., Qian, X., Li, Q., Deng, B., Zhu, Y., Han, Z., Zhang, W., Wang, W., Feng, S.-P., Chen, G., et al. (2020). Giant thermopower of ionic gelatin near room temperature. *Science* 368, 1091–1098. <https://doi.org/10.1126/science.aaz5045>.
- Heyduk, K. (2021). The genetic control of succulent leaf development. *Curr. Opin. Plant Biol.* 59, 101978. <https://doi.org/10.1016/j.pbi.2020.11.003>.
- Hu, L., Hou, J., Ma, Y., Li, H., and Zhai, T. (2016). Multi-heteroatom self-doped porous carbon derived from swim bladders for large capacitance supercapacitors. *J. Mater. Chem. A.* 4, 15006–15014. <https://doi.org/10.1039/C6TA06337C>.
- Hulicova-Jurcakova, D., Seredych, M., Lu, G.Q., and Bandosz, T.J. (2009). Combined effect of nitrogen- and oxygen-containing functional groups of microporous activated carbon on its electrochemical performance in supercapacitors. *Adv. Funct. Mater.* 19, 438–447. <https://doi.org/10.1002/adfm.200801236>.
- Jin, H., Li, J., Yuan, Y., Wang, J., Lu, J., and Wang, S. (2018). Recent Progress in biomass-derived electrode materials for high volumetric performance supercapacitors. *Adv. Energy Mater.* 8, 1801007. <https://doi.org/10.1002/aenm.201801007>.
- Kang, D., Liu, Q., Gu, J., Su, Y., Zhang, W., and Zhang, D. (2015). Egg-box" assisted fabrication of porous carbon with small mesopores for high rate electric double layer capacitors. *ACS Nano* 9, 150929193027001. <https://doi.org/10.1021/acsnano.5b04821>.
- Kim, B., Park, J., Baik, S., and Lee, J.W. (2020). Spent coffee derived hierarchical porous carbon and its application for energy storage. *J. Porous Mater.* 27, 451–463. <https://doi.org/10.1007/s10934-019-00826-7>.
- Li, Y., Dong, J., Zhang, J., Zhao, X., Yu, P., Jin, L., and Zhang, Q. (2015). Nitrogen-doped carbon membrane derived from polyimide as free-standing electrodes for flexible supercapacitors. *Small* 11, 3476–3484. <https://doi.org/10.1002/sml.201403575>.
- Li, Y., Wang, G., Wei, T., Fan, Z., and Yan, P. (2016). Nitrogen and sulfur co-doped porous carbon nanosheets derived from willow catkin for supercapacitors. *Nano Energy* 19, 165–175. <https://doi.org/10.1016/j.nanoen.2015.10.038>.
- Li, Y., Zhao, Y., Cheng, H., Hu, Y., Shi, G., Dai, L., and Qu, L. (2012). Nitrogen-doped graphene quantum dots with oxygen-rich functional groups. *J. Am. Chem. Soc.* 134, 15–18. <https://doi.org/10.1021/ja206030c>.
- Lin, H.B., Huang, W.Z., Rong, H.B., Hu, J.N., Mai, S.W., Xing, L.D., Xu, M.Q., Li, X.P., and Li, W.S. (2015). Surface natures of conductive carbon materials and their contributions to charge/discharge performance of cathodes for lithium ion batteries. *J. Power Sourc.* 287, 276–282. <https://doi.org/10.1016/j.jpowsour.2015.04.077>.
- Liu, X., Ma, C., Li, J., Zielinska, B., Kalenczuk, R.J., Chen, X., Chu, P.K., Tang, T., and Mijowska, E. (2019). Biomass-derived robust three-dimensional porous carbon for high volumetric performance supercapacitors. *J. Power Sourc.* 412, 1–9. <https://doi.org/10.1016/j.jpowsour.2018.11.032>.
- Lou, X., Wen, G., Buyuan, X., and Le, W.Y. (2015). Formation of yolk-shelled Ni-Co mixed oxide nanoprisms with enhanced electrochemical performance for hybrid supercapacitors and lithium ion batteries. *Adv. Energy Mater.* 5, 1500981. <https://doi.org/10.1002/aenm.201500981>.
- Maye, S., Girault, H., and Peljo, P. (2020). Thermally regenerative copper nanoslurry flow battery for heat-to-power conversion with low-grade thermal energy. *Energy Environ. Sci.* 13, 2191–2199. <https://doi.org/10.1039/D0EE01590C>.
- Meng, T., and Xuan, Y. (2020). Enhancing conversion efficiency and storage capacity of a thermally self-chargeable supercapacitor. *Adv. Mater. Inter.* 7, 2000934. <https://doi.org/10.1002/admi.202000934>.
- Meng, T., Xuan, Y., and Zhang, X. (2021). A thermally chargeable hybrid supercapacitor with high power density for directly Converting heat to electricity. *ACS Appl. Energy Mater.* 4, 6055–6061. <https://doi.org/10.1021/acsaem.1c00905>.
- Ming, Z., Lan, J., Xuan, Z., Gang, S., and Yang, X. (2017). Porous carbon derived from *Ailanthus altissima* with unique honeycomb-like microstructure for high-performance supercapacitors. *New J. Chem.* 41, 4281–4285. <https://doi.org/10.1039/C7NJ01127J>.
- Ogburn, R.M., and Edwards, E.J. (2010). The ecological water-use strategies of succulent plants. *Adv. Bot. Res.* 55, 179–225. <https://doi.org/10.1016/B978-0-12-380868-4.00004-1>.
- Pan, F., Cao, Z., Zhao, Q., Liang, H., and Zhang, J. (2014). Nitrogen-doped porous carbon nanosheets made from biomass as highly active electrocatalyst for oxygen reduction reaction. *J. Power Sourc.* 272, 8–15. <https://doi.org/10.1016/j.jpowsour.2014.07.180>.
- Roychowdhury, S., Biswas, R.K., Dutta, M., Pati, S.K., and Biswas, K. (2019). Phonon localization and entropy driven point defects lead to ultralow thermal conductivity and enhanced thermoelectric performance in (SnTe)_{1-2x}(SnSe)_x(SnS)_x. *ACS Energy Lett.* 4, 9b01093. <https://doi.org/10.1021/acse-nergylett.9b01093>.
- Snoeyink, V.L., and Weber, W.J. (1967). The surface chemistry of active carbon; a discussion of structure and surface functional groups. *Environ. Sci. Technol.* 1, 228–234. <https://doi.org/10.1021/es60003a003>.
- Szabó, T., Berkesi, O., Forgó, P., Josepovits, K., and Sanakis, Y. (2006). Evolution of surface functional groups in a series of progressively oxidized graphite oxides. *Chem. Mater.* 18, 2740–2749. <https://doi.org/10.1021/cm060258+>.
- Wang, J., Ding, B., Hao, X., Xu, Y., Wang, Y., Shen, L., Dou, H., and Zhang, X. (2016a). A modified molten-salt method to prepare graphene electrode with high capacitance and low self-discharge rate. *Carbon* 102, 255–261. <https://doi.org/10.1016/j.carbon.2016.02.047>.
- Wang, L., Wei, T., Sheng, L., Jiang, L., Wu, X., Zhou, Q., Yuan, B., Yue, J., Liu, Z., and Fan, Z. (2016b). "Brick-and-mortar" sandwiched porous carbon building constructed by metal-organic framework and graphene: ultrafast charge/discharge rate up to 2Vs⁻¹ for supercapacitors. *Nano Energy* 30, 84–92. <https://doi.org/10.1016/j.nanoen.2016.09.042>.
- Xiao, Z., Mei, Y., Yuan, S., Mei, H., Xu, B., Bao, Y., Fan, L., Kang, W., Dai, F., Wang, R., et al. (2019). Controlled hydrolysis of metal-organic frameworks: hierarchical Ni/Co-layered double hydroxide microspheres for high-performance supercapacitors. *ACS Nano* 13, 7024–7030. <https://doi.org/10.1021/acsnano.9b02106>.
- Xie, P., Yuan, W., Liu, X., Peng, Y., Yin, Y., Li, Y., and Wu, Z. (2021). Advanced carbon nanomaterials for state-of-the-art flexible supercapacitors. *Energy Storage Mater.* 36, 56–76. <https://doi.org/10.1016/j.ensm.2020.12.011>.

Zhang, J., Deng, Y., Wu, Y., Xiao, Z., Liu, X., Li, Z., Bu, R., Zhang, Q., Sun, W., and Wang, L. (2022). Chemically coupled 0D-3D hetero-structure of Co₉S₈-Ni₃S₄ hollow spheres for Zn-based supercapacitors. *Chem. Eng. J.* *430*, 132836. <https://doi.org/10.1016/j.cej.2021.132836>.

Zhang, L., Kim, T., Li, N., Kang, T.J., Chen, J., Pringle, J.M., Zhang, M., Kazim, A.H., Fang, S., Haines, C., et al. (2017). High power density electrochemical thermocells for inexpensively harvesting low-grade thermal energy. *Adv.*

Mater. *29*, 1605652. <https://doi.org/10.1002/adma.201605652>.

Zhang, Q., Han, K., Li, S., Ming, L., Li, J., and Ke, R. (2018). Synthesis of garlic skin-derived 3D hierarchical porous carbon for high-performance supercapacitors. *Nanoscale* *10*, 2427. <https://doi.org/10.1039/C7NR07158B>.

Zhao, D., Wang, H., Khan, Z.U., Chen, J., Gabrielsson, R., Jonsson, M.P., Berggren, M., and

Crispin, X. (2016). Ionic thermoelectric supercapacitors. *Energy Environ. Sci.* *9*, 1450–1457. <https://doi.org/10.1039/C6EE00121A>.

Li, Z., Xu, Z., Tan, X., Wang, H., Holt, C.M., Stephenson, T., Olsen, B.C., and Mitlin, D. (2013). Mesoporous nitrogen-rich carbons derived from protein for ultra-high capacity battery anodes and supercapacitors. *Energy Environ. Sci.* *6*, 871–878. <https://doi.org/10.1039/C2EE23599D>.

STAR★METHODS

KEY RESOURCES TABLE

REAGENT or RESOURCE	SOURCE	IDENTIFIER
Chemicals, peptides, and recombinant proteins		
Potassium hydroxide(KOH)	Aladdin Ltd.	CAS: 1310-58-3
Hydrochloric acid (HCl)	Nanjing Chemical Reagent Co., Ltd.	CAS: 7647-01-0
Polytetrafluoroethylene (PTFE)	Aladdin Ltd.	CAS:9002-84-0
N-methyl-2-pyrrolidone (NMP)	Nanjing Chemical Reagent Co., Ltd.	CAS: 872-50-4
Lithium Sulfate Monohydrate (Li ₂ SO ₄ ·H ₂ O)	Aladdin Ltd.	CAS: 10102-25-7
Sulphuric acid (H ₂ SO ₄)	Nanjing Chemical Reagent Co., Ltd.	CAS: 7664-93-9
Software and algorithms		
Origin 2021	Graphing and data analysis software	https://www.originlab.com/
Other		
Electrochemical workstation	Chinstruments	CHI760E
Electrochemical workstation	Zahner	Zennium Pro
Freeze Dryer	Beijing Science and Technology Development Co., Ltd. Yaxing Instrument Technolog	LGJ-10FD
Battery test system	Land	CT3001A
Transmission electron microscope	Thermo scientific	FEI Talos F200S
Micropore analyzer	Micromeritics	ASAP 2460
X-ray diffraction	Bruker	D8 Advance
X-ray photoelectric spectroscopy	Thermo scientific	ESCALAB 250Xi
Emission scanning electron microscope	Zeiss	GeminiSEM 300

RESOURCE AVAILABILITY

Lead contact

Further information and requests for resources and reagents should be directed to and will be fulfilled by the lead contact, Yimin Xuan (ymxuan@nuaa.edu.cn).

Materials availability

This study did not generate new unique reagents.

Date and code availability

Original data reported in this paper will be shared by the lead contact upon request.

This paper does not report original code.

Any additional information required to reanalyze the data reported in this paper is available from the lead contact upon request.

EXPERIMENTAL MODEL AND SUBJECT DETAILS

The type of succulent plant used in this article is *Crassula arborescens* (Mill.) Willd. Fresh *Crassula arborescens* (Mill.) Willd plants were purchased from the flower market in Jiangsu Province which was identified by Chinese Virtual Herbarium, the collection code is SZG SZG00027546. The succulent plants from one to five years old were respectively selected as the precursors.

METHOD DETAILS

Synthesis of porous carbon materials

KOH and HCl were purchased from Aladdin Ltd. and Nanjing Chemical Reagent Co., Ltd., respectively. The chemical reagents used in this article are used directly without further processing.

The fresh *Crassula arborescens* (Mill.) Willd. plant leaves were ultrasonically cleaned with distilled water and ethanol for half an hour to remove impurities on the surface of the leaves before freeze-drying, after which, the dried blades were preliminarily carbonized under Ar at 600°C for 1 h. The obtained carbon powder was ball-milled and labelled as C-700. The C-700 and KOH are mixed with 15 mL of distilled water according to the mass ratio of 1:2, 1:3 and 1:4, respectively. Then the mixed product stood still at room temperature for 18 h before drying at 60°C for 12 h. The dried mixtures were further activated under Ar at 700°C for 2 h, and finally treated with 1 M HCl aqueous solution. After centrifugation, the product was repeatedly washed with deionized water and ethanol until it became neutral. For simplicity, the obtained products were labeled C-2-700, C-3-700, and C-4-700, respectively.

Material characterizations

The microstructure and morphology of carbon materials were characterized by a field emission scanning electron microscope (SEM, Zeiss, GeminiSEM 300) and transmission electron microscope (TEM, Thermo scientific, FEI Talos F200S). The specific surface area and porosity of the material were measured by the micropore analyzer (ASAP 2460), and calculated by the Brunauer emmett teller (BET) method and the density functional theory method. X-ray diffraction (XRD, Bruker, D8 Advance) with Cu-K α radiation ($\lambda = 1.5418 \text{ \AA}$), Raman spectrum (Horiba LabRAM HR Evolution) and X-ray photoelectric spectroscopy (XPS, Thermo scientific, ESCALAB 250Xi) were devoted to investigate the structure of the porous carbon materials.

Electrochemical measurements of electrodes

The working electrode was prepared from a mixture of the obtained carbon materials, conductive carbon black and binder polytetrafluoroethylene (PTFE) with the mass ratio of 80:15:5. The mixture was dissolved in *n*-methyl-2-pyrrolidone solution and pasted onto graphite paper with a mass loading of 2.0 mg cm⁻². Then, the electrode was dried at 60°C for 12 h. A three-electrode test system was adopted to employ the platinum electrode and saturated calomel electrode as the counter electrode and the reference electrode, respectively, and the electrolyte was 1 M H₂SO₄. CHI760E electrochemical workstation was applied to perform cyclic voltammetry (CV) test and galvanostatic charge and discharge (GCD) test of the working electrode. The Zahner electrochemical workstation was utilized to obtain the AC impedance curve of the working electrode, using the frequency range from 0.01 Hz to 10 KHz in an open circuit state. The cycling stability of the working electrode was tested using the Land battery test system.

The gravimetric capacitances of the C-4-700 working electrode were obtained from the discharge curve of GCD, and the calculation equation was as follows in the three-electrode test system:

$$C_s = \frac{I\Delta t}{m\Delta V} \quad (\text{Equation 1})$$

where C_s (F g⁻¹) represent the gravimetric capacitances of the C-4-700 working electrode, I (A), Δt (s), m (g) and ΔV (V) represent for the discharging current, the time for discharge, the mass of active carbon materials and the width of the potential window, respectively.

The gravimetric specific capacitance of carbon electrode materials can also be calculated by two-electrode system, and the equation used is as follows:

$$C_s = \frac{4I\Delta t}{m\Delta V} \quad (\text{Equation 2})$$

where m (g) represents the mass of positive and negative active materials. And the energy density and power capability of the system can be obtained from:

$$E = \frac{1}{8}C_s V^2 \quad (\text{Equation 3})$$

$$P = \frac{E}{\Delta t} \quad (\text{Equation 4})$$

where E is the voltage of the beginning of the discharging process, Δt is the discharging time span.

QUANTIFICATION AND STATISTICAL ANALYSIS

Our study does not include statistical analysis or quantification.